参赛学生姓名：王涵峥、刘泓森、戴德翔

中学：广州暨大港澳子弟学校

省份：广东省

国家/地区：中国

指导老师姓名：黄振辉、李海玲

指导老师单位：广州暨大港澳子弟学校、广西科技师范学院

论文题目：Multiplicative trichotomous noise induced stochastic resonance in the fractional harmonic oscillator with time delay

2026 Sir Yau High School Science Award
仅用于2026丘成桐中学科学奖论文公示

Multiplicative trichotomous noise induced stochastic resonance in the fractional harmonic oscillator with time delay

Hanzhen Wang, Hongsen Liu, Dexiang Dai

Abstract.

Generalized stochastic resonance (GSR) is investigated for a fractional-order harmonic oscillator with time-delayed damping, subject to multiplicative trichotomous noise. To quantitatively characterize the systems output response to weak periodic forcing, we derive an exact analytical expression for the output amplitude by applying the generalized Shapiro-Loginov formula together with Laplace transform. Numerical analysis indicates that trichotomous noise can induce various resonance behaviors, including inverse SR, bona fide SR, periodic multiresonance and stochastic multiresonance phenomena. Fractional memory, time delay, and damping coefficient substantially shape the resonance characteristics, whereas noise parameters govern the magnitude and shift of resonant peaks. Different parameter combinations produce distinct resonance evolution scenarios and enable switching among various resonance regimes. Monte Carlo parameter sampling validates the obtained analytical solutions and further reveals the underlying regulatory mechanisms of fractional memory and time delay in stochastic resonance dynamics.

Keywords: Stochastic resonance; Trichotomous noise; Time delay; Monte Carlo

1 Introduction and background

In recent decades, exploring how stochastic noise modulates the dynamical behaviors of fractional-order systems has remained an active research topic in nonlinear dynamics and statistical mechanics. Stochastic resonance (SR), first proposed by Benzi et al.[1, 2] in studies of paleoclimatic glacial cycles, describes a counterintuitive nonlinear effect: moderate-intensity noise can amplify a system's response to weak periodic signals, arising from the constructive coupling between noise fluctuations and periodic excitation.

Early SR research mainly focused on integer-order nonlinear systems driven by Gaussian

2026 S.-T. Yau High School Science Award
仅用于2026丘成桐中学科学奖公示

white noise. Subsequent work revealed that linear or fractional-order systems with non-Gaussian colored noise can also exhibit typical SR characteristics[3–7], Benefiting from its unique noise-enhanced weak-signal detection property, SR has been widely applied in practical fields, including weak signal extraction and amplification[8–10], mechanical fault diagnosis[11–13], biological regulatory dynamics[14–16], and anomalous transport of charged particles [17–19]. Traditional SR is defined based on bistable systems, but subsequent research has expanded it to generalized stochastic resonance (GSR)[20, 21]. GSR is characterized by the non-monotonic variation of key quantitative indicators (spectral amplification, signal-to-noise ratio, autocorrelation functions) with system or noise parameters, which does not require the system to be bistable. This generalization greatly enriches the connotation and application scope of SR theory.

Fractional-order calculus provides an effective mathematical tool to describe memory effects and non-local characteristics ubiquitous in real physical systems (such as viscoelastic materials, biological tissues, and complex circuits)[22–25]. Compared with integer-order systems, fractional-order time-delayed damping systems can more accurately simulate the dynamic evolution of actual systems with memory, delay, and damping coupling effects[26–28]. In natural environments, random fluctuations are mostly non-Gaussian colored noise rather than ideal Gaussian white noise. Among various non-Gaussian noises, generalized Mittag-Leffler (GML) noise[29–31], with Mittag-Leffler correlation decay properties, is widely used to describe anomalous diffusion and non-Markovian relaxation processes [32–36]. Trichotomous noise [37–41], as a three-state Markovian noise, can better characterize the complex random fluctuations in real systems than dichotomous noise. The work of [42] theoretically explores the occurrence of SR within a bistable system that incorporates both time delay and trichotomous noise. Reference [43] explores SR in fractional-order oscillators with time delay and fluctuating damping, aiming to clarify the distinct roles played by the two memory sources: time delay and fractional-order damping. Tian Yan et al[44]. investigated SR in fractional-order resonators featuring both time delay and mass fluctuation.

Therefore, it is critically important to investigate the combined effects of damping coefficient, inertia coefficient fluctuations, and time delay, through both theoretical analysis and experimental validation. The rest of the paper is organized as follows. Sec. 2 establishes the fractional-order time-delayed damping system model and presents the basic theoretical framework. In Sec. 3, the SR induced by trichotomous noise is explored, and the respective roles of system-related and noise-related parameters in modulating the resonance response are elucidated. Sec. 4 provides numerical simulations to corroborate the validity of the analytical results. Sec. 5 summarizes the main conclusions.

2026 S. T. Yau High School Science Award
仅用于2026丘成桐中学科学奖论文公示

2 System model and theoretical derivation

2.1 System model

Considering practical viscoelastic vibration systems with memory characteristics and delayed feedback restoring force, we first establish the deterministic fractional-order damped delay dynamic equation under weak periodic external excitation without random fluctuations:

$$ {}_0^C D_t^\delta x(t) + \alpha \ddot{x}(t) + \beta \dot{x}(t) + w_0^2 x(t-\tau) = A\cos(\Omega t),\ (0 < \delta \leq 1) \tag{1} $$

where the Caputo fractional derivative ${}_0^C D_t^\delta x(t)$ describes the hereditary memory effect of viscoelastic materials. α, β and w_0^2 separately denote inertial coefficient, damping coefficient and inherent linear stiffness coefficient, τ stands for the delay time of feedback displacement, and $Acos(\Omega t)$ represents the low-amplitude harmonic driving signal.

Nevertheless, actual operating environments inevitably contain unpredictable random fluctuations: random parametric perturbation modulates the intrinsic stiffness coefficient, and non-Markovian ambient disturbance is superimposed on the external excitation term. To incorporate such two kinds of stochastic perturbations into the deterministic model, we introduce trichotomous multiplicative noise $\zeta(t)$ for random stiffness fluctuation and zero-mean internal fractional Gaussian white noise $\eta(t)$. Consequently, the corresponding fractional harmonic oscillator with time delay equation is rewritten as

$$ {}_0^C D_t^\delta x(t) + \alpha \ddot{x}(t) + \beta \dot{x}(t) + \left(w_0^2 + \zeta(t)\right) x(t-\tau) = A\cos(\Omega t) + \eta(t),\ (0 < \delta \leq 1) \tag{2} $$

The trichotomous noise $\zeta(t)$ is a three-state Markovian multiplicative noise, randomly taking values $-\sigma$, σ and 0, where $\sigma > 0$ is the noise intensity. Its statistical properties satisfy

$$ \langle \zeta(t) \rangle = 0, \quad \langle \zeta(t+\epsilon)\zeta(t) \rangle = 2q\sigma^2 e^{-\lambda\epsilon}, \quad 0 < q \leq \frac{1}{2}, $$

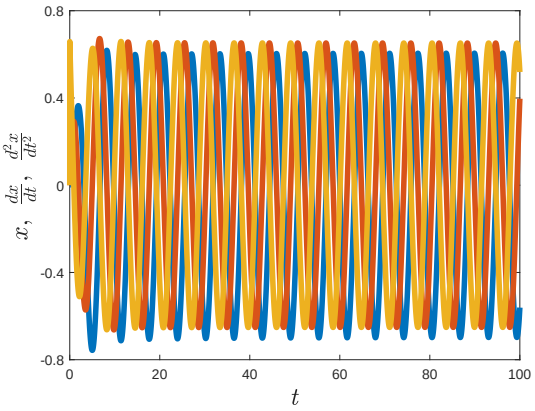
where $\lambda > 0$ is the noise correlation rate, and q is the probability parameter. Compared with dichotomous noise, this noise is more consistent with complex random fluctuations in real systems.

For numerical simulation, Eq. (1) is rewritten in the state-space form:

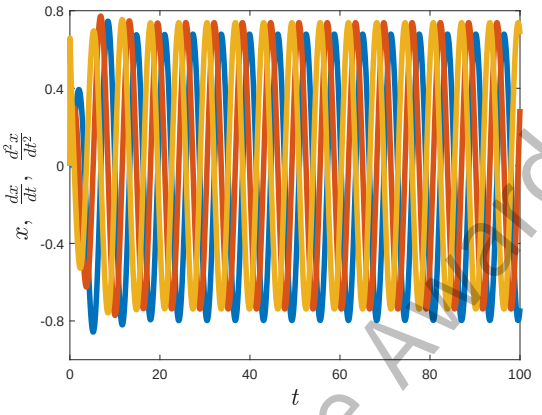
$$ \begin{cases} \dot{x} = y, \\ \dot{y} = z, \\ {}_0^C D_t^\delta x(t) = -\alpha z - \beta y - w_0^2 x(t-\tau) + A\cos(\Omega t) \end{cases} \tag{3} $$

Fig. 1 presents the time-domain evolution of the system under noise-free conditions. In each subplot, the blue curve represents displacement $x(t)$, the orange curve denotes velocity $\dot{x}(t)$,

2026 S.T. Yau High School Science Award
仅用于2026丘成桐中学科学奖论文公示



(a)



(b)

Fig. 1: **(a)** $x, \frac{dx}{dt}, \frac{d^2x}{dt^2}$ versus t, for $\delta = 0.3, \tau = 0.4$. **(b)** $x, \frac{dx}{dt}, \frac{d^2x}{dt^2}$ versus t, for $\delta = 0.8, \tau = 0.8$. Other parameter values: $\alpha = 1.5, \beta = 1.8, \Omega = 1,\ \omega_0 = 1,\ A = 1$.

and the yellow curve corresponds to acceleration $\ddot{x}(t)$. It is observed that the three state variables undergo periodic oscillations with small amplitudes in the initial stage. When comparing Fig. 1(a) and (b), one can observe distinct steady-state oscillation amplitudes under the two groups of fractional order δ and time delay τ. These deterministic time-domain responses serve as a baseline reference for the subsequent investigation of noise-induced generalized stochastic resonance.

2.2 Analytical derivation of output amplitude

To quantitatively characterize the generalized stochastic resonance behavior of the fractional-order time-delayed system, output amplitude is selected as the quantitative evaluation index. Based on the generalized Shapiro-Loginov moment-preserving formula for fractional stochastic systems and Laplace transform [45], the analytical expression of the output amplitude is derived.

For the trichotomous Markovian noise $\zeta(t)$, the generalized Shapiro-Loginov moment-retention formula is adopted to evaluate the time derivative of noise-response correlation terms, which reads:

$$\frac{\mathrm{d}}{\mathrm{d}t}\langle\zeta^i(t)\Phi(\zeta)\rangle = \lambda\langle\zeta^i(t)\rangle\langle\Phi(\zeta)\rangle + \langle\zeta^i(t)\frac{\mathrm{d}}{\mathrm{d}t}\Phi(\zeta)\rangle - \lambda\langle\zeta^i(t)\Phi(\zeta)\rangle, \tag{4}$$

in which $\Phi(\zeta)$ represents a function of the stochastic process ζ. Taking an ensemble average of Eq. (2) yields:

$$ {}_0^C D_t^\delta\langle x(t)\rangle + \alpha\langle\ddot{x}(t)\rangle + \beta\langle\dot{x}(t)\rangle + \omega_0^2\langle x(t-\tau)\rangle + \langle\zeta(t)x(t-\tau)\rangle = A\cos(\Omega t). \tag{5}$$

2026 Sixth Yau High School Science Award
仅用于2026丘成桐中学科学奖论文公示

There is a new correlator $\langle\zeta x(t-\tau)\rangle$ in Eq. (5). Therefore, one can derive the following equation after multiplying Eq. (2) by $\zeta(t)$ and averaging:

$$\langle\zeta(t)D^{\delta}x\rangle+\alpha\langle\zeta\frac{\mathrm{d}^2x}{\mathrm{d}t^2}\rangle+\beta\langle\zeta\frac{\mathrm{d}}{\mathrm{d}t}x\rangle+\omega_0^2\langle\zeta x(t-\tau)\rangle+\langle\zeta^2x(t-\tau)\rangle=0 \tag{6}$$

Using formula (4)[30, 46], one finds

$$\langle\zeta\frac{\mathrm{d}}{\mathrm{d}t}x\rangle=\lambda\langle\zeta x\rangle+\frac{\mathrm{d}\langle\zeta x\rangle}{\mathrm{d}t}, \tag{7}$$

$$\langle\zeta\frac{\mathrm{d}^2x}{\mathrm{d}t^2}\rangle=\frac{\mathrm{d}^2}{\mathrm{d}t^2}\langle\zeta x\rangle+2\lambda\frac{\mathrm{d}\langle\zeta x\rangle}{\mathrm{d}t}+\lambda^2\langle\zeta x\rangle. \tag{8}$$

Using formula (4) and the definition of Caputo fractional derivative, one readily obtains

$$\langle\zeta(t)D^{\delta}x\rangle=e^{-\lambda t}D^{\delta}(\langle\zeta(t)x(t)\rangle e^{\lambda t}). \tag{9}$$

A new correlator $\langle\zeta^2x(t-\tau)\rangle$ arises in Eq.(6). The following results can be derived after multiplying Eq. (2) by $\zeta^2(t)$ and using the properties $\zeta^3(t)=\sigma^2\zeta(t)$ and $\langle\zeta^2(t)\rangle=2q\sigma^2$:

$$\left\langle\zeta^2(t)D^{\delta}x\right\rangle+\alpha\langle\zeta^2\frac{\mathrm{d}^2x}{\mathrm{d}t^2}\rangle+\beta\langle\zeta^2\frac{\mathrm{d}x}{\mathrm{d}t}\rangle+\omega_0^2\langle\zeta^2x(t-\tau)\rangle+\sigma^2\langle\zeta x(t-\tau)\rangle=2q\sigma^2A\cos(\Omega t) \tag{10}$$

Using the Eq. (4) again [30, 46]:

$$\frac{\mathrm{d}\langle\zeta^2x\rangle}{\mathrm{d}t}=\langle\zeta^2\frac{\mathrm{d}x}{\mathrm{d}t}\rangle+2q\sigma^2\lambda\langle x\rangle-\lambda\langle\zeta^2x\rangle, \tag{11}$$

$$\langle\zeta^2\frac{\mathrm{d}^2x}{\mathrm{d}t^2}\rangle=\lambda^2\langle\zeta^2x\rangle+\frac{\mathrm{d}^2}{\mathrm{d}t^2}\langle\zeta^2x\rangle+2\lambda\frac{\mathrm{d}}{\mathrm{d}t}\langle\zeta^2x\rangle-4q\sigma^2\lambda\frac{\mathrm{d}}{\mathrm{d}t}\langle x\rangle-2q\sigma^2\lambda^2\langle x\rangle. \tag{12}$$

According to the definition of the Caputo fractional derivative, we have

$$\left\langle\zeta^2(t)D^{\delta}x\right\rangle=\frac{1}{\Gamma(1-\delta)}\int_0^t\frac{\langle\zeta^2(t)\dot{x}(u)\rangle}{(t-u)^{\delta}}du. \tag{13}$$

From the Shapiro-Loginov formula, we obtain

$$\left\langle\zeta^2(t)D^{\delta}x\right\rangle=2q\sigma^2D^{\delta}\langle x\rangle+e^{-\lambda t}D^{\delta}\left[\left(\langle\zeta^2(t)x(t)\rangle-2q\sigma^2\langle x(t)\rangle\right)e^{\lambda t}\right]. \tag{14}$$

For convenient computation, we assume $X_1(s)$, $X_2(s)$ and $X_3(s)$ are the Laplace transforms of $\langle x(t)\rangle$, $\langle\zeta(t)x(t-\tau)\rangle$ and $\langle\zeta^2(t)x(t-\tau)\rangle$, respectively. By applying the final-value theorem of the Laplace transformation in the long-time limit, the initial conditions of $\langle x(t)\rangle$, $\langle\zeta(t)x(t)\rangle$ and $\langle\zeta^2(t)x(t)\rangle$ will vanish. Taking the Laplace transforms of Eqs. (5),(6), (10), and combining Eqs. (7),(8), (9), (11),(12), (14), we obtain

$$\begin{aligned}
&d_1(s)X_1(s)+e^{-s\tau}X_2(s)=\frac{As}{s^2+\Omega^2},\\
&d_2(s)X_2(s)+e^{-s\tau}X_3(s)=0,\\
&d_3(s)X_1(s)+\sigma^2e^{-s\tau}X_2(s)+d_2(s)X_3(s)=2q\sigma^2\frac{As}{s^2+\Omega^2},
\end{aligned} \tag{15}$$

2026 S.-T. Yau High School Science Award 仅用于2026丘成桐中学科学奖论文公开

where

$$
\begin{aligned}
d_1(s) &= s^\delta + \alpha s^2 + \beta s + w_0^2 e^{-s\tau}, \\
d_2(s) &= (s+\lambda)^\delta + \alpha(s+\lambda)^2 + \beta(s+\lambda) + \omega_0^2 e^{-s\tau}, \\
d_3(s) &= 2q\sigma^2[s^\delta - (s+\lambda)^\delta - \alpha\lambda(2s+\lambda) - \beta\lambda],
\end{aligned} \tag{16}
$$

Solving algebraic Eq. (15), one can obtain

$$
X_1(s) = \tilde{H}(s)\frac{As}{s^2+\Omega^2}, \tag{17}
$$

where

$$
\tilde{H}(s) = \frac{d_2^2(s) + e^{-2s\tau}\sigma^2(2q-1)}{d_1(s)(d_2^2(s) - \sigma^2 e^{-2s\tau}) + e^{-2s\tau}d_3(s)}.
$$

For the sake of stable solution, the following inequality holds:

$$
\sigma^2 < \frac{\omega_0^2\left(\lambda^\delta + \alpha\lambda^2 + \beta\lambda + \omega_0^2\right)^2}{\omega_0^2 + 2q\left(\lambda^\delta + \alpha\lambda^2 + \beta\lambda\right)} \tag{18}
$$

The stationary first moment of system Eq. (2) can be obtained by the linear response theory. Therefore, the stationary first moment $\langle x(t)\rangle_{as}$ can be written as

$$
\langle x(t)\rangle_{as} = A\int_0^t H(t-u)\cos(\Omega u)\mathrm{d}u = A_{st}\cos(\Omega t + \varphi). \tag{19}
$$

in which $H(t)$ is the inverse Laplace transform of $\tilde{H}(s)$. The amplitude A_{st} and the phase shift φ in Eq. (19) are written as

$$
\begin{cases}
A_{st} = A\sqrt{\frac{f_1^2+f_2^2}{f_3^2+f_4^2}}, \\
\varphi = \arctan(\frac{f_2 f_3 - f_1 f_4}{f_1 f_3 + f_2 f_4}),
\end{cases} \tag{20}
$$

where

$$
\begin{aligned}
f_1 &= f_5^2 - f_6^2 + \sigma^2(2q-1)\cos(2\Omega\tau), \\
f_2 &= 2f_5 f_6 + \sigma^2(2q-1)sin(2\Omega\tau), \\
f_3 &= f_{11}f_7 - f_{12}f_8 + cos(2\Omega\tau)f_9 - sin(2\Omega\tau)f_{10}, \\
f_4 &= f_{11}f_8 + f_{12}f_7 + cos(2\Omega\tau)f_{10} + sin(2\Omega\tau)f_9,
\end{aligned} \tag{21}
$$

2026 S.-T. Yau High School Science Award
仅用于2026丘成桐中学科学奖论文公示

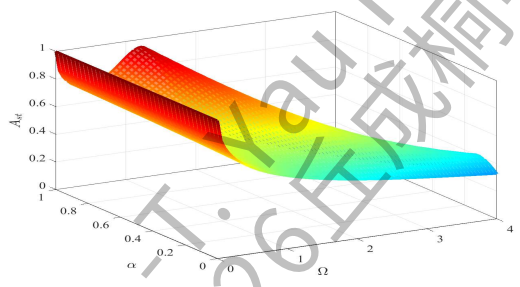
in which

$$
\begin{aligned}
f_5 &= \left(\lambda^2+\Omega^2\right)^{\frac{\delta}{2}}\cos\left(\delta\arctan\frac{\Omega}{\lambda}\right)+\alpha\left(\lambda^2-\Omega^2\right)+\beta\lambda+w_0^2\cos(\Omega\tau),\\
f_6 &= -\left(\lambda^2+\Omega^2\right)^{\frac{\delta}{2}}\sin\left(\delta\arctan\frac{\Omega}{\lambda}\right)-2\alpha\lambda\Omega-\beta\Omega+w_0^2\sin(\Omega\tau),\\
f_7 &= f_5^2-f_6^2-\sigma^2\cos(2\Omega\tau),\\
f_8 &= 2f_5f_6-\sigma^2 sin(2\Omega\tau),\\
f_9 &= 2q\sigma^2\left[\Omega^\delta\cos\left(\frac{\pi\delta}{2}\right)-\left(\lambda^2+\Omega^2\right)^{\frac{\delta}{2}}\cos\left(\delta\arctan\frac{\Omega}{\lambda}\right)-\alpha\lambda^2-\beta\lambda\right],\\
f_{10} &= 2q\sigma^2\left[-\Omega^\delta\sin\left(\frac{\pi\delta}{2}\right)+\left(\lambda^2+\Omega^2\right)^{\frac{\delta}{2}}\sin\left(\delta\arctan\frac{\Omega}{\lambda}\right)+2\alpha\lambda\Omega\right],\\
f_{11} &= \Omega^\delta\cos\left(\frac{\pi\delta}{2}\right)-\alpha\Omega^2+\omega_0^2 cos(\Omega\tau),\\
f_{12} &= -\Omega^\delta\sin\left(\frac{\pi\delta}{2}\right)-\beta\Omega+\omega_0^2 sin(\Omega\tau).
\end{aligned}
\tag{22}
$$

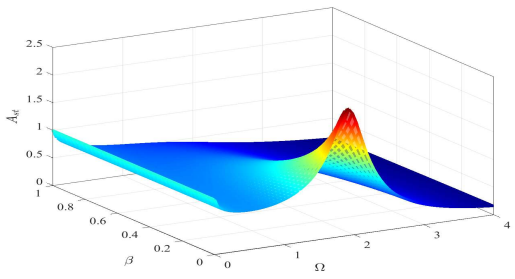
3 SR phenomenon induced by trichotomous noise

We will focus on studying the GSR of the output amplitude A_{st} by discussing the trichotomous noise parameters ($\sigma,\ q,\ \lambda$) and the system parameters($\alpha,\ \beta$, δ, ω_0 and τ). Our work primarily discusses the stochastic resonance phenomenon of the output amplitude with respect to system parameters and noise parameters.

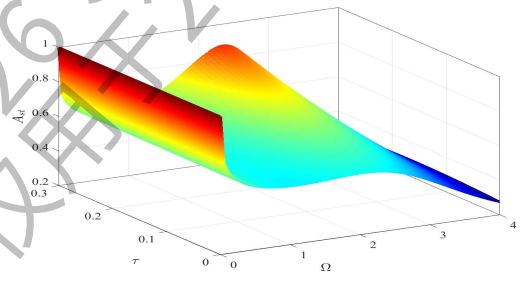
3.1 The influence of system parameters on resonance behavior



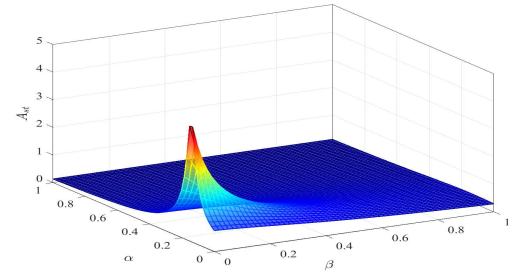
(a)



(b)

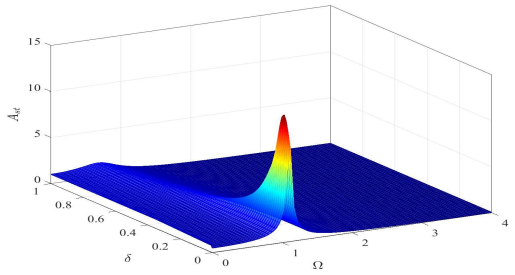


(c)

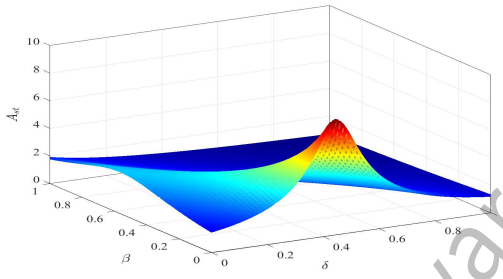


(d)

2026 S.-T. Yau High School Science Award
仅用于2026丘成桐中学科学奖论文公示



(e)



(f)

Fig. 2: **(a)** 3D A_{st} distribution in the (α, Ω) plane with $\beta = 0.5$, $\tau = 0.3$, and $\delta = 0.5$; **(b)** 3D A_{st} profile in the (β, Ω) space with $\alpha = 0.5$, $\tau = 0.3$, and $\delta = 0.5$; **(c)** 3D A_{st} plot in the (τ, Ω) space with $\alpha = 0.3$, $\beta = 0.5$, and $\delta = 0.3$; **(d)** 3D A_{st} distribution in the (α, β) space with $\delta = 0.5$, $\Omega = 3$, and $\tau = 0.5$; **(e)** 3D A_{st} distribution in the (δ, Ω) space with $\alpha = 1.5$, $\beta = 0.5$, and $\tau = 0.6$; **(f)** 3D A_{st} distribution in the (β, δ) space with $\Omega = 1$, $\alpha = 1.5$, and $\tau = 0.6$. other parameter values:$\lambda = 0.1$, $\omega_0 = 1$, $q = 0.1$, $\sigma = 0$, $A = 1$.

In this subsection, the GSR phenomenon is investigated as a function of system parameters. Fig. 2 demonstrates three-dimensional graphs of output amplitude A_{st}. Fig. 2(a) presents A_{st} as a function of the inertial parameter α and the excitation frequency Ω. A_{st} maintains a high output amplitude in the low-frequency region and forms a distinct resonance peak at moderate values of Ω. As the excitation frequency increases further, the A_{st} decays steadily and remains at low levels in the high-frequency band, illustrating the frequency-dependent modulation effect of α on the GSR behavior of the system.

Fig. 2(b) depicts A_{st} as a function of the damping parameter β and the excitation frequency Ω. An isolated resonance peak appears for $1 < \Omega < 3$, whereas A_{st} remains extremely low elsewhere in the parameter space. This suggests that GSR emerges when the damping parameter and driving frequency are optimally matched.

Fig. 2(c) presents the A_{st} as a function of the time delay τ and the excitation frequency Ω. A_{st} maintains a high output amplitude at small τ and low Ω, forming a clear resonance peak near moderate Ω. As Ω gradually increases, the output amplitude initially decays sharply, and a clear resonance peak emerges around $\Omega = 2$, at which point the system response significantly enhanced. Subsequently, as Ω is further increased, A_{st} rapidly decays and remains at a very low level.

Fig. 2(d) shows the A_{st} as a function of the inertial parameter α and damping parameter β. Fig. 2(d) exhibits a resonance peak for the small inertial parameter α and the small damping parameter β. With A_{st} decaying rapidly as α and β deviate from the optimal matching range.

2026 S.-T. Yau High School Science Award
仅用于2026丘成桐中学科学奖论文公示

Fig. 2(e) presents the A_{st} as a function of the fractional order δ and the excitation frequency Ω. A significant and sharp resonance peak appears near $1 < \Omega < 2$, while the influence of A_{st} remains negligible in most other parameter regions.

Fig. 2(f) shows the A_{st} as a function of the damping parameter β and the fractional order δ. A smooth and prominent bell-shaped resonance peak emerges at $\delta = 0.5$, with A_{st} decaying rapidly as the parameters deviate from the optimal matching region.

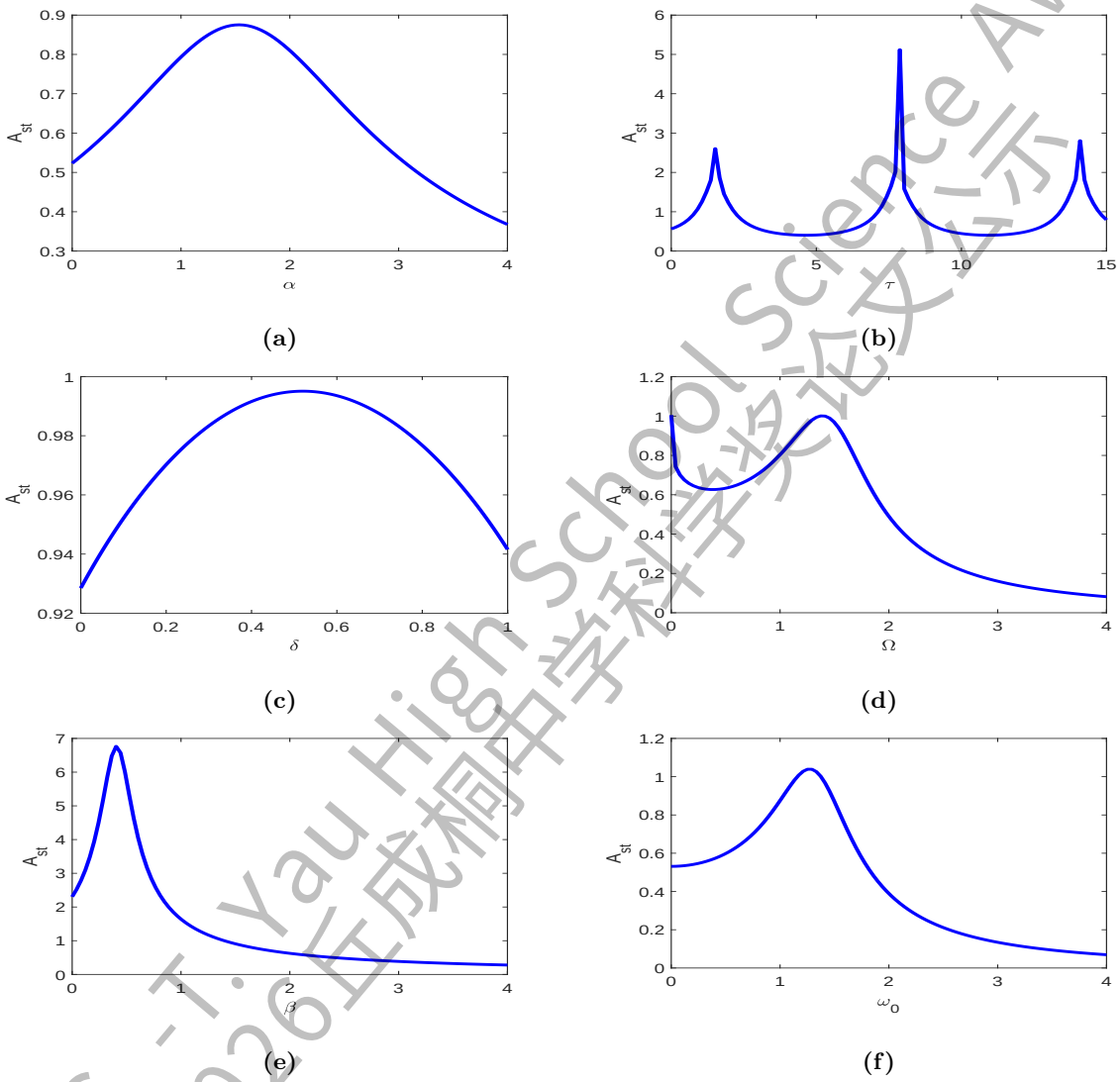


Fig. 3: A_{st} obtained from Eq. (20) as functions of different parameters: **(a)** vs. α, with $\beta = 1$, $\delta = 0.5$, $\tau = 0.6$, $\Omega = 1$, $\sigma = 0$, $\omega_0 = 1$; **(b)** vs. τ, with $\alpha = 0.8$, $\beta = 0.8$, $\delta = 0.5$, $\Omega = 1$, $\sigma = 0.6$, $\omega_0 = 1$; **(c)** vs. δ, with $\alpha = 0.8$, $\beta = 0.6$, $\tau = 0.8$, $\Omega = 1$, $\sigma = 1.5$, $\omega_0 = 1$; **(d)** vs. Ω, with $\alpha = 0.8$, $\beta = 0.8$, $\tau = 0.5$, $\delta = 0.3$, $\sigma = 0.2$, $\omega_0 = 1$; **(e)** vs. β, with $\alpha = 1.5$, $\tau = 0.8$, $\delta = 0.2$, $\Omega = 1$, $\sigma = 0$, $\omega_0 = 1$; **(f)** vs. ω_0, with $\alpha = 1.5$, $\beta = 1$, $\tau = 0.6$, $\delta = 0.5$, $\sigma = 0$, $\Omega = 1$. Common parameters: $\lambda = 0.1$, $A = 1$, $q = 0.1$.

Fig. 3 displays the GSR behaviors of A_{st} varying with different system parameters. Fig. 3(a) exhibits a single smooth resonance peak of A_{st} with respect to the inertial parameter α, and A_{st}

2026 S.-T. Yau High School Science Award 仅用于2026丘成桐中学科学奖公示

decays beyond the optimal resonant interval. Fig. 3(b) illustrates multiple resonance peaks of A_{st} as a function of time delay τ, exhibiting the typical multi-peak resonance characteristic. Fig. 3(c) shows the effect of the fractional-order parameter δ on the single peak of A_{st}. As δ increases, the value of A_{st} first rises and then falls, peaking significantly within the range $0.3 < \delta < 0.6$. Fig. 3(d) presents the resonance curve of A_{st} as a function of the excitation frequency Ω. Within the range $0 < \Omega < 2$, the curve exhibits both a distinct valley and a subsequent peak. As Ω increases from zero, the A_{st} value initially drops to a minimum, indicating a region of suppressed response. Following this trough, the curve rises sharply to a maximum before gradually declining again. This phenomenon confirms the bona fide stochastic resonance as defined by Gammaitoni. Fig. 3(e) illustrates the resonance curve of A_{st} as a function of the damping coefficient β. It can be observed that a single peak emerges within the range of $0 < \beta < 1$, indicating that an optimal damping level exists for maximizing the system response. Beyond this optimal point, further increase in β suppresses the output amplitude. Fig. 3(f) presents the resonance curve of A_{st} versus the inherent linear stiffness coefficient ω_0. A single peak is clearly observed, indicating that the system attains its maximum vibrational amplitude at a specific stiffness value, beyond which the response gradually declines.

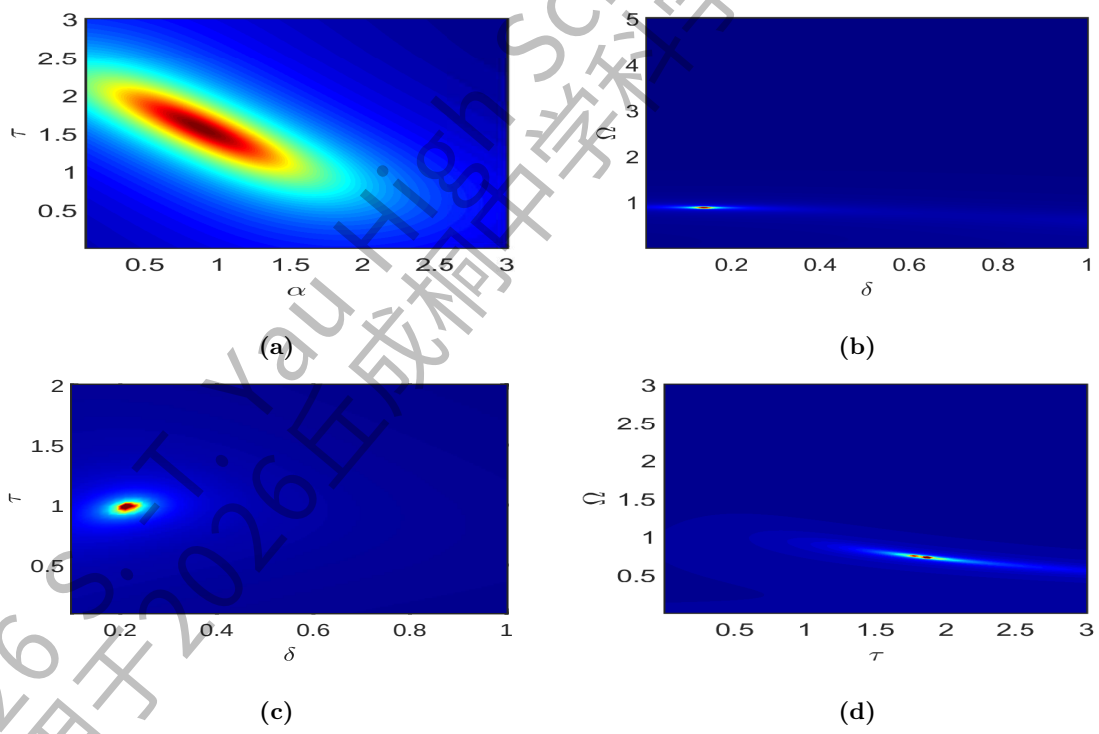


Fig. 4: **(a)** α versus τ, for $\beta = 0.8,\ \delta = 0.3,\ \Omega = 1$. **(b)** δ versus Ω, for $\alpha = 2.2,\ \beta = 0.5,\ \tau = 0.8$. **(c)** δ versus τ, for $\alpha = 1.5,\ \beta = 0.5,\ \Omega = 1$. **(d)** τ versus Ω, for $\alpha = 1.5,\ \beta = 0.5,\ \delta = 0.5$. Other parameter values: $\lambda = 0.1, \omega_0 = 1, \sigma = 0,\ q = 0.1,\ A = 1$.

Fig. 4 depicts the contour distribution of GSR behavior of A_{st} as a function of coupled system parameters. Fig. 4(a) shows the high-intensity resonant response region between the

2026 S.T. Yau High School Science Award 仅用于2026丘成桐中学科学奖公示

inertial parameter α and time delay τ.The region presents an elongated concentrated hotspot and reflects a strong synergistic resonance coupling effect. Fig. 4(b) illustrates discrete localized resonant hotspots in the parameter plane of fractional order δ and excitation frequency Ω. Only a narrow, single resonant band emerges at low excitation frequency, while the amplitude decays rapidly as Ω increases, showing that resonance can be excited only within a limited frequency region can under given fractional-order conditions. Fig. 4(c) displays an obvious centralized resonance peak in the $\delta - \tau$ plane. A_{st} reaches its maximum at the optimal matching pair of δ and τ, and the resonant response gradually weakens outside this central parameter region. As shown in Fig. 4(d), the resonance region is extremely narrow, and the resonance disappears immediately once the parameters are detuned. This indicates that the resonance exhibits poor robustness, as even a slight parameter mismatch can completely suppress the resonant behavior.

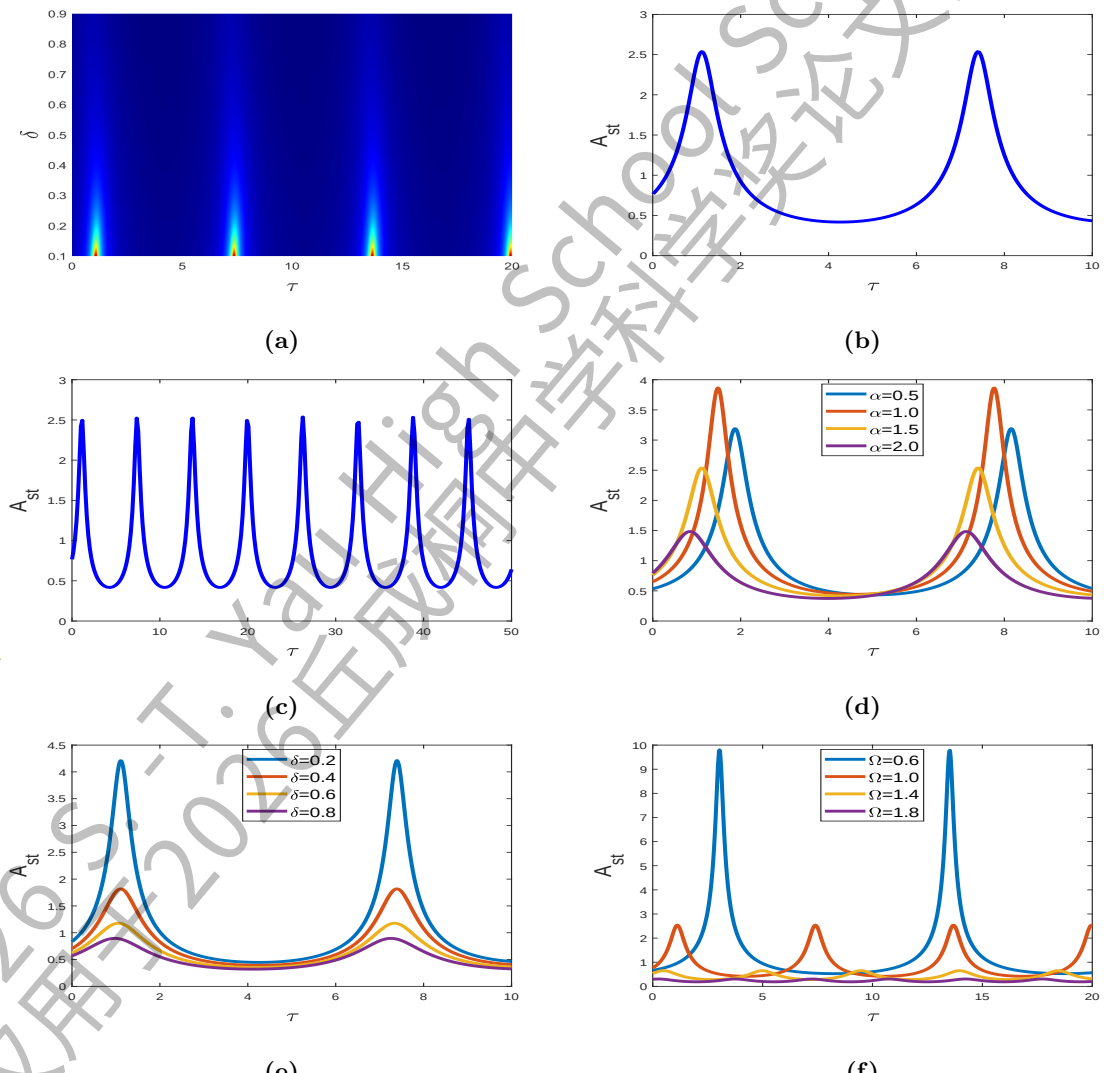


Fig. 5: **(a)** τ versus δ, for $\alpha = 1.5,\ \Omega = 1$. **(b)-(f)** of A_{st} versus τ. **(b)** $\alpha = 1.5,\ \delta = 0.3,\ \Omega = 1$; **(c)** $\alpha = 1.5,\ \delta = 0.3,\ \Omega = 1$; **(d)** $\delta = 0.3,\ \Omega = 1$; **(e)** $\alpha = 1.5,\ \Omega = 1$); **(f)** $\alpha = 1.5,\ \delta = 0.3$. Other parameter values: $\beta = 0.8,\ \lambda = 0.1,\ \omega_0 = 1,\ \sigma = 0,\ q = 0.1,\ A = 1$.

2026 S.-T. Yau High School Science Award
仅用于2026丘成桐中学科学奖论文公示

Combined with the analytical solutions derived from Eq. (20), the parameter-dependent behavior of the output amplitude A_{st} is illustrated in Fig. 5. As shown in Fig. 5(a), the fractional order δ exerts a monotonic inhibitory effect on the resonance intensity. At smaller values of δ, the system exhibits weak dissipative effects, and the superposition of time-delay phases can excite intense resonance, with the amplitude showing sharp peaks. As δ increases, the fractional order dissipation strengthens, and the resonance amplitude decays rapidly. When $\delta > 0.3$, no significant resonance is observed across the entire time-delay range. This result indicates that adjusting the fractional-order exponent can effectively modulate the time-delay-induced resonance intensity, providing a parameter-tuning basis for vibration suppression and resonance enhancement.

Fig. 5(b) shows the dynamic behaviors of A_{st} as a function of τ. Two peaks and one valley are presented. With all other parameters held constant, increasing τ from its value in Fig. 5(b) yields the outcomes presented in Fig. 5(c). This reveals a clear periodic multi-resonance pattern. The response exhibits evenly spaced, nearly equal-amplitude resonance peaks separated by stable low-amplitude valleys, characteristic of SMR.

Fig. 5(d) exhibits the representative generalized stochastic resonance behaviors of A_{st} as a function of the time delay τ for various values of α. It can be observed from the figure that two resonance peaks emerge, and as α increases, the peak values of these resonances first rise and then decline.

Fig. 5(e) illustrates the representative generalized stochastic resonance behavior of A_{st} as a function of time delay τ under different δ values. From the figure, it can be observed that two resonance peaks appear, and as the δ value increases, the peak amplitude of the resonance peaks decreases.

Fig. 5(f) exhibits the representative generalized stochastic resonance behaviors of A_{st} as a function of the time delay τ under different values of Ω. It can be observed from the figure that as Ω increases, periodic resonance occurs. It can also be seen from the graph that increasing Ω leads to a decrease in resonance intensity.

3.2 The influence of noise parameters on resonance behavior

In this subsection, we will mainly investigate GSR behavior in Eq. (20) under the influence of noise parameters. Fig. 6 depicts the resonant behavior of A_{st} with respect to the noise intensity σ. As shown in Fig. 6(a), a distinct resonance peak emerges for $0 < \sigma < 3$. In Fig. 6(b), when β is increased while keeping all other parameters unchanged, a resonance peak also appears; however, its amplitude is considerably suppressed compared to that observed in Fig. 6(a). This

2026 S.-T. Yau High School Science Award
仅用于2026丘成桐中学科学奖论文公示

reduction indicates that a larger β tends to weaken the resonant response, suggesting that β serves as a modulating factor in the stochastic resonance mechanism. A single-peak stochastic resonance phenomenon is observed in Fig. 6(c). In Fig. 6(d), all parameters are identical to those in Fig. 6(c) except for an increased Ω, and a similar unimodal resonance is observed. This consistency indicates that the resonant behavior persists under changes in Ω, though the peak position and amplitude may be modulated by this parameter.

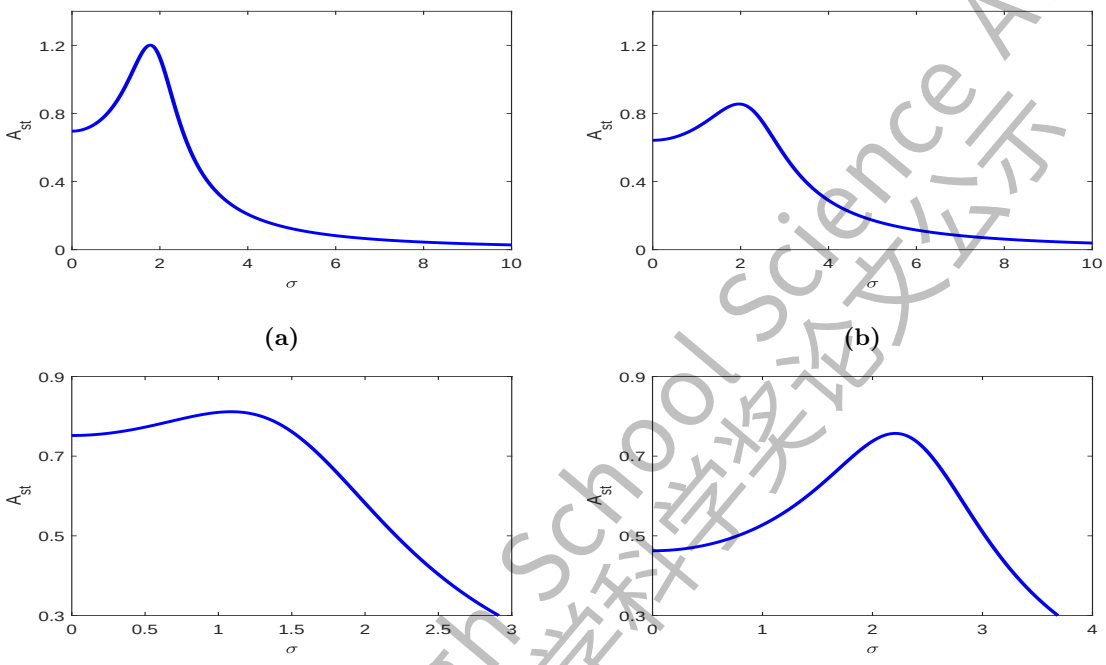
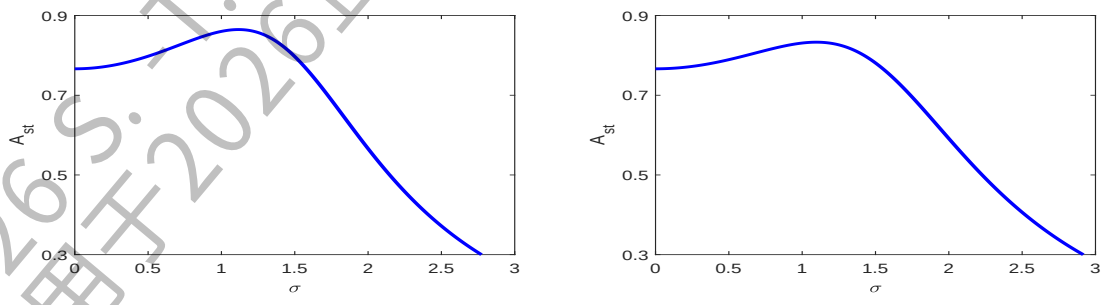
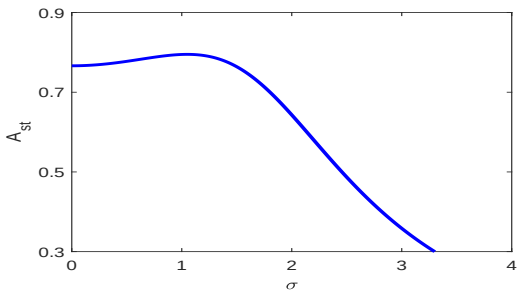


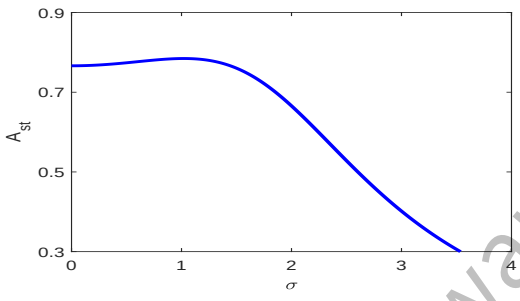
Fig. 6: Resonance of the output amplitude A_{st} as function of σ. **(a)** $\alpha = 0.2$, $\omega_0 = 1$, $\Omega = 1$, $\beta = 0.5$, $\tau = 0.3$, $\delta = 0.5$, $\lambda = 1$, $q = 0.5$, $A = 1$; **(b)** the same parameters as **(a)**, except that $\beta = 1.5$; **(c)** $\alpha = 0.2$, $\omega_0 = 1$, $\Omega = 1.7$, $\beta = 0.5$, $\tau = 0.8$, $\delta = 0.8$, $\lambda = 1$, $q = 0.5$, $A = 1$; **(d)** the same parameters as **(c)**, except that $\Omega = 2.3$.



2026 S. T. Yau High School Science Award
仅用于2026丘成桐中学科学奖论文公示



(c)



(d)

Fig. 7: Resonance of the output amplitude A_{st} as function of σ. **(a)** $\alpha = 0.2$, $\omega_0 = 0.6$, $\Omega = 1$, $\beta = 0.8$, $\tau = 1.6$, $\delta = 0.6$, $\sigma = 2$, $q = 0.5$, $A = 1$,$\lambda = 0.8$; **(b)** the same parameters as **(a)**, except that $\lambda = 1$; **(c)** the same parameters as **(a)**, except that $\lambda = 1.5$; **(d)** the same parameters as **(a)**,except that $\lambda = 1.8$.

Resonance peaks are present in Fig. 7(a)-(d). As the parameter λ increases, the amplitude of the resonance peak gradually decreases while the peak position shifts to the right. When λ exceeds a certain threshold, the resonance peak completely disappears, indicating that this parameter exerts a suppressive effect on the system's resonance characteristics.

4 Monte Carlo Sampling over Noise Parameter Space

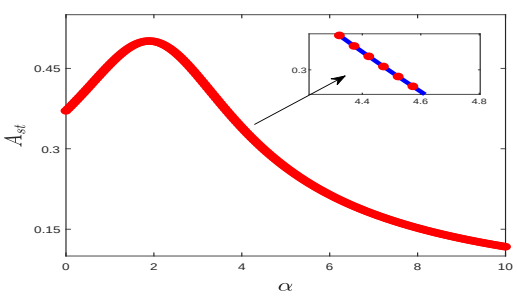
To further investigate how parametric fluctuation affects the stochastic phase approximation, we use random sampling to characterize the statistical properties of the system [43, 44, 47]. To verify the analytical predictions and explore the statistical features of resonance behaviors induced by fluctuations in noise intensity, sampling tests are carried out. The noise intensity parameter σ is modeled as a Gaussian random variable:

$$\sigma = \sigma_0 + \sigma_1 \xi, \quad \xi \sim \mathcal{N}(0, 1) \tag{23}$$

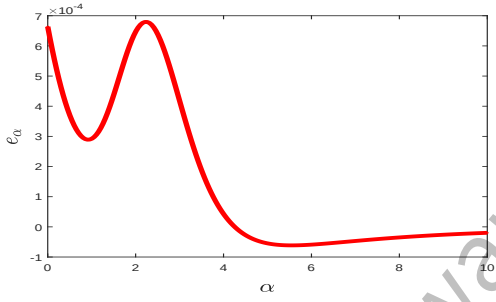
where σ_0 is the mean value and σ_1 is the fluctuation amplitude. A lower bound $\sigma \geq \sigma_{min}$ is imposed to avoid unphysical negative values.

A total of $N = 500$ independent stochastic realizations are generated. For each realization, the steady-state amplitude A_{st} is evaluated using the analytical formula. The ensemble-averaged amplitude A_{st} is obtained by averaging over all realizations and is used to validate the theoretical predictions.

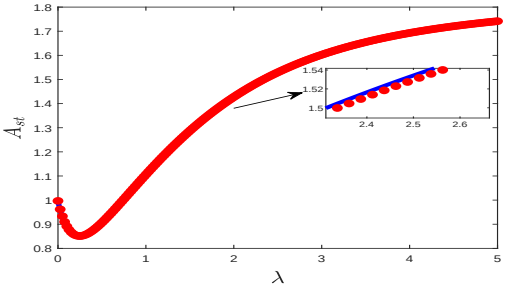
2026 S. T. You High School Science Award
仅用于2026丘成桐中学科学奖论文公示



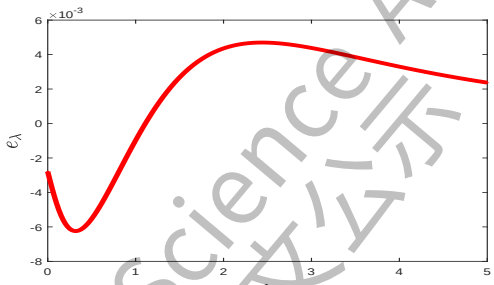
(a)



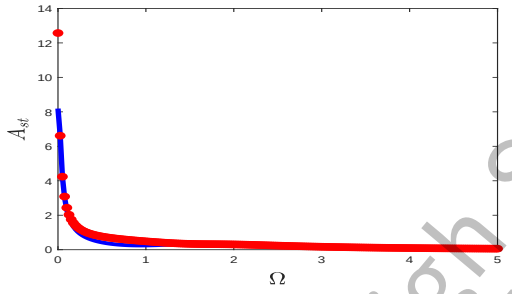
(b)



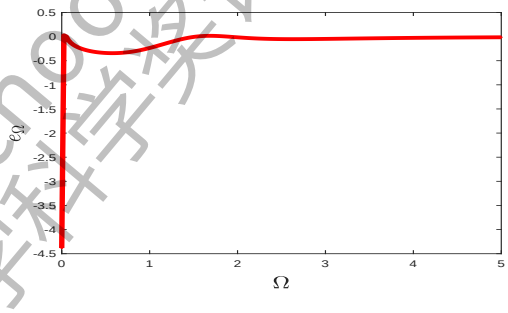
(c)



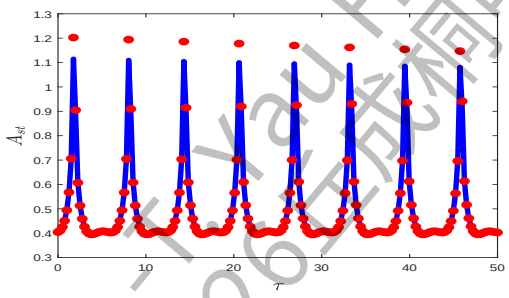
(d)



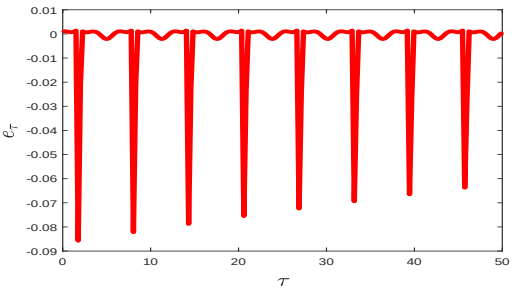
(e)



(f)



(g)



(h)

2026 S. Yau High School Science Award
仅用于2026年成功申请科学奖论文公示

Fig. 8: Comparison between the analytical and numerical results for A_{st} with respect to α, λ, Ω and τ, along with the corresponding numerical deviation graphs. **(a)** α: $\lambda = 0.8,\ \Omega = 1,\ \omega_0 = 1,\ \beta = 1.5,\ \tau = 0.5,\ \delta = 0.5,\ q = 0.25,\ \sigma = 1.8,\ A = 1$; **(b)** the same parameters as **(a)**; **(c)** λ: $\alpha = 1.5,\ \Omega = 1,\ \omega_0 = 1,\ \beta = 0.5,\ \tau = 0.5,\ \delta = 0.3,\ q = 0.25,\ \sigma = 1.8,\ A = 1$; **(d)** the same parameters as **(c)**; **(e)** Ω: $\lambda = 0.1,\ \alpha = 0.8,\ \omega_0 = 1,\ \beta = 1.8,\ \tau = 0.5,\ \delta = 0.5,\ q = 0.2,\ \sigma = 1.5,\ A = 1$; **(f)** the same parameters as **(e)**; **(g)** τ: $\lambda = 0.1,\ \Omega = 1,\ \omega_0 = 1,\ \beta = 1.5,\ \alpha = 0.5,\ \delta = 0.2,\ q = 0.4,\ \sigma = 1.2,\ A = 1$; **(h)** the same parameters as **(g)**. Blue solid lines are analytical results from Eq. (20), and red markers denote Monte Carlo ensemble-averaged values.

As shown in Fig. 8(a), the steady-state output amplitude A_{st} against parameter α, exhibiting a standard unimodal stochastic resonance curve peaking at $\alpha \approx 2$. The inset verifies the high consistency between analytical solutions and numerical data. In Fig. 8(b) depicts the numerical deviation e_α between the numerical results and theoretical values. The error reaches its maximum near $\alpha = 2$ and gradually decays to zero as α increases. The similar trends of A_{st} and e_α reveal that the numerical deviation is closely related to the resonant response modulated by α.

Fig. 8(c)-(d) illustrate the variation of steady-state amplitude A_{st} and the numerical deviation e_λ against parameter λ. Fig. 8(c) shows a typical anti-resonance curve of A_{st}: it drops rapidly to a minimum for small λ, then increases monotonically and slowly approaches a constant plateau as λ increases. Meanwhile, the discrete simulation points agree well with the analytical curve. Fig. 8(d) plots the numerical deviation e_λ between analytical solutions and Monte Carlo parameter sampling results. The deviation reaches its largest negative value at the same small λ that corresponds to the anti-resonance valley, and gradually decays to near zero with increasing λ. The consistent positions of the anti-resonance trough and maximum numerical deviation indicate that the mismatch between simulation and theory is significantly amplified under the anti-resonance condition modulated by λ.

Fig. 8(e)-(f) depict the steady-state amplitude A_{st} and the numerical deviation e_Ω as functions of the driving frequency Ω. A_{st} attains its maximum at $\Omega = 0$ and decays rapidly, while the discrete simulation points align closely with the analytical curve. Meanwhile, the numerical deviation reaches its maximum negative value at $\Omega = 0$, fluctuates weakly afterward and slowly converges to zero at large Ω, demonstrating that the greatest mismatch between theory and simulation emerges at low driving frequencies.

As shown in Fig. 8(g), periodic multi-peak stochastic resonance responses of the steady-state output amplitude A_{st} are observed as a function of time delay τ. As τ increases, resonance peaks recur periodically with slightly decaying magnitudes. The analytical curves agree well with the

2026 S.-T. Yau High School Science Award
仅用于2026丘成桐中学科学奖公示

numerical results. Fig. 8(h) plots numerical deviation e_τ between numerical and theoretical solutions. The error fluctuates near zero in non-resonance intervals and forms obvious negative spikes at each resonance position of τ. The consistent periodic positions of resonance peaks and error spikes demonstrate that numerical deviation reaches its maximum at each resonant state modulated by time-delay parameter τ.

All curves are numerically evaluated from Eq. (20), with blue solid lines representing analytical results and red dots denoting Monte Carlo parameter sampling outcomes. The figure exhibits excellent agreement between theoretical predictions and sampling results.

5 Conclusion

This paper investigates the GSR in a fractional-order time-delayed damping system driven by trichotomous multiplicative noise. The Shapiro-Loginov formula is utilized to obtain the precise analytical expression for the output amplitude A_{st}. The impacts of time delay τ, noise intensity σ, and noise correlation rate λ on resonance behavior were also analyzed. To verify the accuracy of our analytical results, we perform Monte Carlo parameter sampling. These sampling results corroborate the reliability of our theoretical findings and demonstrate the practical relevance of the present work. The main results are summarized as follows:

First, trichotomous multiplicative noise can induce GSR in the system, exhibiting bona fide SR, reverse SR, periodic multiresonance, and stochastic multiresonance phenomena.

Second, stochastic multi-resonance and periodic resonance are observed in the output amplitude A_{st} versus time delay τ. Increasing δ and Ω suppresses resonance intensity, and increasing Ω leads to periodic resonances. Additionally, a single-peak resonance is found versus noise intensity σ, and a valley appears versus noise correlation rate λ.

Finally, Monte Carlo parameter sampling verifies the theoretical results and confirms the effectiveness of the analytical approach. These findings offer a theoretical foundation for weak signal processing within fractional-order systems.

2026 S.-T. Yau High School Science Award
仅用于2026丘成桐中学科学奖论文公示

References

[1] Benzi, Roberto, Alfonso Sutera, and Angelo Vulpiani. "The mechanism of stochastic resonance." Journal of Physics A: mathematical and general 14.11 (1981): L453-L457.

[2] Gammaitoni L , Jung P , Marchesoni F ,et al.Stochastic resonance [Review][J].Reviews of Modern Physics, 1998(1):70.

[3] M. Gitterman, Classical harmonic oscillator with multiplicative noise, Phys. A, 352 (2005) 309-334.

[4] K. Wiesenfeld, F. Moss, Stochastic resonance and the benefits of noise: from ice ages to crayfish and squids, Nature, 373 (1995) 33-36.

[5] L. Gammaitoni, A.R. Bulsara, Noise activated nonlinear dynamic sensors, Phys. Rev. Lett, 88 (2002) 230601.

[6] Migliorini, Giuliano, and Duccio Fanelli. "Multiplicative noise induced bistability and stochastic resonance." Journal of Physics: Complexity 5.4 (2024): 045001.

[7] Han, Ping, et al. "Semiconductor laser systems excited by multiplicative Ornstein-Uhlenbeck noise and additive sine-Wiener noise in relation to real and imaginary parts." Physical Review E 109.6 (2024): 064126.

[8] M.E. Inchiosa, A.R. Bulsara, L. Gammaitoni, Higher-order resonant behavior in asymmetric nonlinear stochastic systems, Phys. Rev. E, 55 (1997) 4049C4056.

[9] Y. Wang, S. Jiao, Q. Zhang, L. Shuang, X. Qiao, A weak signal detection method based on adaptive parameter-induced tri-stable stochastic resonance, Chin. J. Phys, 56 (2018) 1187-1198.

[10] W. Cheng, X. Xu, Y. Ding, K. Sun, Q.Q. Li, L. Dong, An adaptive smooth unsaturated bistable stochastic resonance system and its application in rolling bearing fault diagnosis, Chin. J. Phys, 65 (2020) 629-641.

[11] G. Zhang, Y. Zhang, T. Zhang, R. Mdsohel, Stochastic resonance in an asymmetric bistable system driven by multiplicative and additive Gaussian noise and its application in bearing fault detection, Chin. J. Phys, 56 (2018) 1173-1186.

[12] Y. Mao, L. Du, W. Guo, D. Mei, Effects of self-propulsion, chirality and noise-correlation on the entropic stochastic resonance of an active Brownian particle, Chin. J. Phys, 65 (2020) 54-63.

[13] Mi, Li-Na, et al. "Stochastic resonance in gene transcriptional regulatory system driven by Gaussian noise and Lvy noise." Chaos, Solitons & Fractals 167 (2023): 113096.

[14] I. Goychuk, V.O. Kharchenko, R. Metzler, How molecular motors work in the crowded environment of living cells: coexistence and efficiency of normal and anomalous transport, PloS. one, 9 (2014) e91700.

[15] I. Goychuk, Anomalous transport of subdiffusing cargos by single kinesin motors: the role of mechanoC-chemical coupling and anharmonicity of tether, Phys. Bio, 12 (2015) 016013.

[16] R. Benzi, Stochastic resonance: from climate to biology, Nonlinear Proc Geoph, 17 (2010) 431-441.

[17] N.V. Agudov, A.V. Krichigin, D. Valenti, B. Spagnolo, Stochastic resonance in a trapping overdamped monostable system, Phys. Rev. E, 81 (2010) 051123.

[18] R.N. Mantegna, B. Spagnolo, L. Testa, M. Trapanese, Stochastic resonance in magnetic systems described by Preisach hysteresis model, J. Appl. Phys, 97 (2005) 453.

[19] T. Djurhuus, V. Krozer, Numerical analysis of stochastic resonance in a bistable circuit, Int. J. Circ. Theor. App, 45 (2016) 625-635.

[20] Krishna, Raghav, and Dilip Kumar Choudhary. "Improved Signal Detection in Bistable Systems Through Stochastic Resonance Across Diverse Noise Environments." IEEE Access (2025).

[21] Berdichevsky, V., and M. Gitterman. "Multiplicative stochastic resonance in linear systems: Analytical solution." EPL (Europhysics Letters) 36.3 (1996): 161-166.

[22] C.H. Chang, Y.T. Tsong, Stochastic resonance in a biological motor under complex fluctuations, Phys. Rev. E, 69 (2004) 021914.

[23] G.T. He, Y. Tian, M.K. Luo, Charge-particles transport in semiconductors characterized by a generalized Langevin equation with a fractional noise, Phys. A, 535 (2019) 122339.

[24] G.T. He, G.J. Tang, M.K. Luo, Y. Tian, H. Eugene Stanley, Three transport models for charged particles in three-dimensional semiconductors driven by a fractional noise, Phys. A, 572 (2021) 125876.

[25] G.T. He, G.J. Tang, Y. Tian, M.K. Luo, H. Eugene Stanley, Non-Markovian thermal-bath-induced Brownian motion in velocity space in the presence of a magnetic field at arbitrary direction, J. Stat. Mech, 2 (2021) 023204.

2026 S. Tiyan High School Science Award 仅用于2026年上饶市科学奖公示

[26] Wang, QiuBao, Hao Wu, and YueJuan Yang. “The effect of fractional damping and time-delayed feedback on the stochastic resonance of asymmetric SD oscillator.” Nonlinear Dynamics 107.3 (2022): 2099-2114.

[27] Ren, R., Xia, W., Wang, Z., & Deng, K. (2022). Stochastic resonance of double fractional-order coupled oscillator with mass and damping fluctuations. Physica Scripta, 97(10), 105206.

[28] Yang, J. H., et al. “Stochastic P-bifurcation and stochastic resonance in a noisy bistable fractional-order system.” Communications in Nonlinear Science and Numerical Simulation 41 (2016): 104-117.

[29] G.T. He, D.L. Guo, Y. Tian, T.J. Li, M.K. Luo, Mittag-Leffler noise induced stochastic resonance in a generalized Langevin equation with random inherent frequency, Phys. A, 484 (2017) 91-103.

[30] G.T. He, Y. Tian, M.K. Luo, Mittag-Leffler noise induced resonance behavior in a fractional generalized Langevin equation with random trichotomous inherent frequency, J. Stat. Mech-Theory. E, 3 (2018) 033201.

[31] M. Gitterman, I. Shapiro, Stochastic resonance in a harmonic oscillator with random mass subject to asymmetric dichotomous noise, J. Stat. Phys, 144 (2011) 139-149.

[32] Viales A D , Wang K G ,M. A. Despsito.Anomalous diffusive behavior of a harmonic oscillator driven by a Mittag-Leffler noise[J].American Physical Society, 2009(1).DOI:10.1103/PHYSREVE.80.011101.

[33] Vainstein, Mendeli H., et al. “Non-exponential relaxation for anomalous diffusion.” EPL (Europhysics Letters) 73.5 (2006): 726-732.

[34] Seifi, M., Ebadi, Z., Agahi, H., Mehri-Dehnavi, H., & Mohammadzadeh, H. (2025). Mittag-Leffler quantum statistics and thermodynamic anomalies. Physical Review E, 112(6), 064102.

[35] Metzler, Ralf, and Joseph Klafter. “Anomalous Stochastic Processes in the Fractional Dynamics Framework: Fokker-Planck Equation, Dispersive Transport, and Non-Exponential Relaxation.” Advances in Chemical Physics (2001): 223-264.

[36] Lim, Chan, and Jae-Hyung Jeon. “Anomalous diffusion in coupled viscoelastic media: A fractional Langevin equation approach.” Physical Review Research 7.4 (2025): 043356.

[37] Mankin R, Ainsaar A, Reiter E. Trichotomous noise-induced transitions[J]. Physical Review E, 1999, 60(2): 1374.

[38] Mankin R, Ainsaar A, Haljas A, et al. Trichotomous-noise-induced catastrophic shifts in symbiotic ecosystems[J]. Physical Review E, 2002, 65(5): 051108.

[39] Zhong S, Wei K, Gao S, et al. Trichotomous noise induced resonance behavior for a fractional oscillator with random mass[J]. Journal of Statistical Physics, 2015, 159(1): 195-209.

[40] Guo F, Li H, Liu J. Stochastic resonance in a linear system with random damping parameter driven by trichotomous noise[J]. Physica A: Statistical Mechanics and its Applications, 2014, 409: 1-7.

[41] B.V. Dasarathy, P. Srinivasan, On the study of a third-order mechanical oscillator, J. Sound. Vib, 9 (1969) 49-52.

[42] Zhou B , Lin D .Stochastic resonance in a time-delayed bistable system driven by trichotomous noise[J].Indian Journal of Physics, 2017, 91(3):299-307.

[43] Tian Yan, He Guitian, et al.The impact of memory effect on resonance behavior in a fractional oscillator with small time delay[J].Physica, A. Statistical mechanics and its applications, 2021, 563(1).

[44] Tian Y , Yu T , He G T ,et al. The resonance behavior in the fractional harmonic oscillator with time delay and fluctuating mass[J].Physica A: Statistical Mechanics and its Applications, 2019, 545:123731.

[45] V.E. Shapiro, V.M. Loginov, Formulae of differentiation and their use for solving stochastic equations, Phys. A, 91 (1978) 563-574.

[46] H.L. Li, G.T. He, L.N. Qiu, L.H. Lv, Y. J. Tang, Y. Peng, Resonance behavior for a trapped particle described by a three-dimensional fractional Langevin equation, Res. Phys, 26 (2021) 104296.

[47] Berghaus, Claudia, Angela Hilgers, and Jrgen Schnakenberg. “Monte Carlo and numerical studies of coloured noise and stochastic resonance problems.” Zeitschrift fr Physik B Condensed Matter 100.1 (1996): 157-163.

2026 S-Tyau High School Science Award
仅用于2026年成都中学科学奖论文公示